

LIQUEFACTION OF INDUSTRIAL ZONE AGAINST EARTHQUAKE LOADING USING LABORATORY AND FIELD MEASUREMENTS

Purpose. To assess the liquefaction of Kirkuk's industrial region following a series of earthquakes that struck the city during the previous five years based on the current earthquake activity in the region.

Methodology. Initially, substantial relationships for shear wave velocity in different types of soil were collected and studied, where the majority of these correlations necessitated the use of standard penetration tests in the field. Indeed, two boreholes were drilled up to a maximum depth of 10 m, and the numbers of blows for conventional penetration tests were measured at various depths in each borehole. The stated shear wave velocity values from the literature, as well as the maximum and lowest shear wave velocity constraints, were employed in a simple technique to estimate the cyclic shear stress induced by earthquake loading.

Findings. Based on laboratory and field data, the safety factor against earthquake-induced liquefaction can be determined. When the worst-case scenario was examined using the suggested values of shear wave velocity, the factor of safety against earthquake was reduced by 94 % as the depth increased from 3.5 to 9 m.

Originality. No previous study has tried to quantify the liquefaction impact of industrial zone of Kirkuk city as such an important rich-oil area was influenced by series of earthquakes occurrence. More importantly, for the first time field soil samples from on-site boreholes in Kirkuk city have been collected and used for liquefaction assessment since such real field data can be utilized properly in liquefaction evaluation process in the absence of any comparable quantification for the investigated area.

Practical value. Precious liquefaction analysis should be performed prior to any proposed project construction in the light of increased earthquake activity in the industrial zone in Kirkuk city (Iraq).

Keywords: *liquefaction, standard penetration test, earthquake, shear wave velocity, soil disturbance, factor of safety*

Introduction. The main harm to the foundation of structures was because of the soil liquefaction during the latest earthquakes since such soil liquefaction has caused excessive differential settlements. In addition, liquefaction evaluation of any location is one of the crucial qualities that should be assessed essentially when the area is damaged by successive earthquakes. Hence, it is required to quantify the liquefaction of any area before starting the process of improving the soil or constructing structures. As the effective stress decreases and the pore-water pressure rises, granular materials undergo a phase change from a solid to a liquefied state known as liquefaction. Soil liquefaction might cause sand boiling, differential and total settlements, and flow breakdowns to land collapse where such harms can trigger serious damage to houses, roads, bridges, harbor facilities, and several other components of the life preservers.

Following the Alaskan (1964) and Niigata (1995) earthquakes, liquefaction was the subject of much investigation. Substantial cracks of many buildings have been observed because of the earthquakes in Kobe-Japan (1995), Chi-Chi-Taiwan (1999), Bhuj-India (2001), and Fukushima-Japan (2011) [1]. There are areas exposed to liquefaction since the soil condition is loose and saturated. Static liquefaction in saturated sandy soil has been identified to be one of the largest catastrophic failure processes. As the static liquefaction happens, the soil resistance decreases and the soil layer's capacity to support many uses in geotechnical engineering such as constructing earth dams, bridges, pillars, cliffs, and embankments is decreased. In addition, a theoretical study has been performed to estimate both liquefaction and pore water pressure for saturated sandy soil under the involvement of machine dynamic loading conditions [2].

The study used the finite element method adopting an equivalent linear elastic model for the soil and harmonic loading form for the dynamic applied loads. The results showed that as load amplitude and frequency were increased, deformation and liquefaction occurred more frequently and more severely. An experimental work for the liquefaction of sandy soil under the influence of a small machine model has been conducted [3]. The research has concentrated on varying the

relative density for the sand, the shape and embedment of the footing model. The analysis has shown that the failure can occur beneath the footing model due to the liquefaction in the sandy soil as the resulted settlement can reach 300 % of the width or footing diameter. Another study used field data to investigate the liquefaction of two different locations in Kerbala city, Iraq [4]. The findings have been used to design charts for estimating the liquefaction potential based on the soil relative density.

Ground failure is considered one of the land failures that can happen after severe earthquakes. Liquefaction is a very complicated problem as it may initiate the loss in the shear strength and it has been investigated by many researchers, however; no unique solution has been adopted yet [1]. It was suggested to quantify the average shear stress obtained from the earthquake depending on the grain particle size [5]. The number of blows (N) from the conventional penetration test is another approach used to assess the liquefaction potential. Standard Penetration Test (SPT) is a field test that can be used for sites exposed to earthquakes whether they had faced liquefaction or not. Shear wave velocities and SPT-N values have been demonstrated to correlate reliably, allowing for the prediction of soil liquefaction independent of geographical location. More importantly, a statistical investigation has used both shear and compression wave velocities for 14 selected locations in the middle region of Iraq to obtain different correlations with various soil properties [6].

It is vital to appropriately predict shear wave velocity since the shear velocity in non-cohesive soils with strain level less than 0.001 % is important for the examination and design of miscellaneous geotechnical constructions [7]. Shear wave velocity is a crucial input in finite element systems used for dynamic investigations of structures, the soil-structure interface, and liquefaction potential evaluations. When evaluating the behavior of soil deposits during an earthquake, the dynamic shear modulus is an essential restriction to consider. Every system's capacity for transient response can be primarily determined by the resonance frequency or duration of the vibration. Substantial problems with the earthquake engineering branch such as earthquake motions, soil-structure interface, and wave intensification involve information necessary to solve the shear wave velocity problem in residual soil.

The investigation of studying the possibility of liquefaction in Kirkuk city has become an important issue for several causes, involving economic difficulties, the lack of complete soil information for different regions of Kirkuk city, the recent rise in earthquake destruction, and the absence of a reliable soil database for Kirkuk soils and the variety of soil types found throughout the city.

In general, SPT values were used in evaluation of the soil liquefaction rather than shear wave velocity. Nevertheless, this study used the shear wave velocity in assessing the liquefaction due to several reasons such as the impossibility of obtaining SPT values for different places and various depths in Kirkuk city, unavailability of reliable SPT database for Kirkuk city, prohibited oil zones in Kirkuk city, and difficulty of acquiring field soil data from built-in projects. Indeed, this study investigates the probability of different ranges of shear wave velocity in various soils depending on published mathematical relationships from literature incorporated with SPT values from selected field sites for the current studied area. The variety of the shear wave velocity covers various soil types with all expected earthquake ranges and probable anticipated liquefactions.

The primary aim of this analysis was to predict the liquefaction aptitude of the industrial region at Kirkuk city depending on shear wave correlations integrated with field and laboratory test results. The specific objectives were as follows:

1. Examine the available correlations of the number of blows (N) and shear wave velocity.
2. Collect field data using two boreholes in the industrial region.
3. Analyze the liquefaction using cyclic shear stress attained from the earthquake loading

Shear Wave Measurement. Shear wave velocity numbers vary depending on the measuring techniques, and the lack of a trustworthy reference makes the shear wave velocity exceedingly challenging to confirm that the acquired values are accurate. In order to make the most use of the data, it is necessary to employ specialist tools and techniques know-how to validate the assessment of shear wave velocity.

Any site's fundamental period is calculated as $4H/V_s$ in seconds, where V_s (m/s) is the mean shear wave velocity and H (m) is the layer thickness. V_s is therefore regarded as a significant soil characteristic in seismic and geotechnical works operations in the area close to the ground surface. Additionally, the investigation of wave amplification and soil-structure interaction uses V_s . Systematic techniques are utilized in evaluating soil-structure schemes exposed to vibrating loading and used for low strain magnitude as specified in the field. Shear wave velocity is used in a variety of seismic wave studies, including down-hole, up-hole, seismic cross-hole, and several co-surface wave analyses. The most accurate technique is the seismic cross-hole test that is applied for determining the shear velocity for in situ soil conditions, considerable amount of sediment in-between the holes, and undisturbed soil characteristics. In cross-hole technique, the shear velocity is measured horizontally across the thick strata. The test is normally performed in three neighboring close boreholes with special devices for generating and receiving shear waves where both compression and shear waves are generated by mechanical instruments. Considering the test's effectiveness in measuring shear waves in the soil strata, evaluating seismic data is a time-consuming and complicated method that necessitates the expertise of geophysicists. Both compression and shear waves are produced by hitting both top and bottom of a cylinder at different stages and recording the data at the same level for consistency. The timely influx of compression and shear waves on the seismic records is employed to evaluate the velocity at a specific level.

Well-controlled experiments and field tests measurement depending on detailed research efforts are employed to study the shear wave velocity. Model analysis of surface waves and

spectral analysis of surface waves are two approaches that may be used to quantify shear wave velocity on the spot, and these have contributed to the widespread adoption of in-situ evaluations of shear wave velocities [8].

Normally, SPT is implemented in a particular hole considerably from one point to another and from one depth to another without any limits. Many efforts have been done to correlate the SPT values (N) with several significant soil characteristics that require sampling and testing. Thus, SPT is commonly utilized in calculating soil characteristics including angle of internal friction and relative density. SPT is applied to estimate the soil bearing capacity, settlement, dynamic shear modulus, unconfined compressive strength of soils, and liquefaction possibility of sandy soils. Additionally, SPT is utilized to estimate shear wave velocity using N -values.

Field tests, such as SPT, have been employed in conjunction with shear wave velocity and laboratory measurement to develop shear wave type correlations to capture a wide range of field data [9, 10].

Even though shear wave velocity quantification is favored, correlation with penetration resistance offers economical time contribution for different conditions. These conditions include creating maps for regional ground hazards, liquefaction studies to check the accuracy of shear wave measurement, geophysical measurement as a screening tool, justification in low risk projects that have limited budget in field testing, and evaluating shear wave profile that uses Rayleigh wave testing [11].

It has been shown that many of presently used correlations ignore some important soil factors such as soil type variation, geological age, particle characteristics, and original composition of soil. For instance, shear wave velocity is primarily determined by confining stress and soil void ratio as follows

$$V_s = Af(e)(\sigma_m)^B, \quad (1)$$

where V_s is the shear wave velocity; $f(e)$ is a function dependent on void ratio while A and B are material arbitrary coefficients; σ_m is the effective overburden stress. The constant B varies between 0.22 and 0.29 where the applied B value was found to be 0.25 [12]. The traditional interaction procedure assumes the soil particles to be smooth, elastic spheres and predicted B value to equal 0.16 [13]. However, if the contacts between the grains have rough surface, then the constant B is considered to be closer to experimental values [14].

Normally, the effective stress is converted based on the overburden adjustment value [8]. For vertical effective stress, the shear wave velocity is normalized as follows

$$V_{s1} = V_s \left[\frac{P_a}{\sigma_v} \right]^{0.25}, \quad (2)$$

where V_{s1} is the stress-standardized shear wave velocity while P_a is the normal atmospheric units as σ_v ($P_a = 100$ kPa when σ_v is in kPa).

Substituting (1) into (2), the standardized shear wave velocity is stated as follows

$$V_{s1} = Af(e)(\sigma_m)^B \left[\frac{P_a}{\sigma_v} \right]^{0.25}.$$

As $B = 0.25$, $P_a = 100$ kPa and $\sigma_v = \sigma_m(3/(1 + k_o))$, where k_o is the lateral earth coefficient at the rest condition, then

$$V_{s1} = Af(e) \left[\frac{100}{(3/(1 + 2k_o))} \right]^{0.25}.$$

It is the lowest void ratio that determines the maximum shear wave velocity, which is in the range of 175 to 327 m/s. However, the lowest shear wave velocity corresponding to the highest void ratio ranges from 114 to 214 m/s. The values of minimum and maximum shear wave velocities depend on the variation of soil characteristics, initial fabric and the values of

both minimum and maximum void ratios. It was noted that the difference of the shear wave velocity between the densest and loosest conditions is less than 132 m/s [8]. On the other hand, correlations were found in the literature relating N with shear wave velocity where such relationships have given up to 4010 m/s discrepancy in the shear wave values between the loosest and the densest soil states. The empirical relationships have no functions that take in consideration the grain properties including particle size and shape, particle gradation, and mineral compositions. The SPT data were employed to predict the shear wave velocity as summarized in Table 1. It is obvious that the majority of earlier models used N values in nonlinear power simulations to estimate the shear wave velocity.

Site, Borehole and Geological Description. The studied location lies in the southern industrial region of Kirkuk city in Iraq where two boreholes were excavated with a depth of 10 m measured from the ground surface. The two boreholes are located at coordinates of N35°22.696' E044°18.338' and

N35°22.685' E044°18.331' respectively. The locations of both boreholes 1 and 2 on the google map are shown in Figs. 1, a, b. Since both studied boreholes are close to each other and for the sake of clarity, each of the investigated boreholes was mapped individually in a single image.

The diameter of the drilled boreholes was 120 mm. Data from disturbed area were obtained at different depths of the cuttings whereas undisturbed soil sample were collected by a standard split spoon sampler. In addition, SPT was conducted at the borehole at different distances depending on the soil stratification.

It should be known that the surface structure of Kirkuk city in Iraq is the simply folded zone type extended from the northern area of Iraq and it involves the subdivision of the Zagros Orogenic Belt [26]. Nevertheless, the main large-scale city's structures that incorporate the hydrocarbon supplying sources are not the conventional base created from decollements of the foreland basin deposits. Even though the city's folds alter and distort sediments originated from the Zagros uplands and accumulated into the creating foreland basin, the originated faults are advanced from the pre-Zagros stratigraphy. The borders of Kirkuk city are described by the variations in topography and associated with the structural alterations. The Mountain Front Flexure defines the northeastern limit and related with the imbricated assaults. The upper altitude of the city's folds into the southeast of Lurestan Salient could be resulted by the consequence of the adjacent gradient at the Khanaqin lineament.

Laboratory Testing. The laboratory test has been conducted on the soil samples to evaluate the engineering characteristics of the soil. The laboratory program has been performed satisfying the requirement of the ASTM (American Society for Testing and Materials) standards. The laboratory soil tests include the following:

1. **Classification Tests.** The classification tests are Atterberg limits (liquid and plastic limits-ASTM D 4318-2010), grain size analysis (sieve and hydrometer analysis-ASTM D 422-63) and moisture content (ASTM D 2216).

2. **Consolidation Test.** The tests include evaluating the variations of the overburden pressure and pre-consolidation pressure with depth (ASTM D 2435). The laboratory and field test results for both boreholes Nos. 1 and 2 have been summarized in Tables 2 and 3 respectively. The results of the consolidation test for samples selected from both boreholes 1 and 2 have been summarized in Table 4.

Table 1

Correlation between shear wave velocity and N values

No.	Reference	Relation	Soil Type
1	[15]	$V_s = 22N^{0.76}$	Sandy Soil*
2	[16]	$V_s = 68.3N^{0.292}$	All Soils*
3	[17]	$V_s = 22N^{0.85}$	All Soils*
		$V_s = 19N^{0.85}$	Sandy Soil*
		$V_s = 22N^{0.77}$	Silty Soil*
		$V_s = 27N^{0.73}$	Clayey Soil*
4	[18]	$V_s = 90N^{0.309}$	All Soils*
		$V_s = 90.82N^{0.319}$	Sandy Soil*
		$V_s = 97.89N^{0.269}$	Clayey Soil*
5	[19]	$V_s = 82.6N^{0.43}$	All Soils*
		$V_s = 79N^{0.434}$	Sandy Soil*
6	[20]	$V_s = 137.153N^{0.229}$	All Soils*
		$V_s = 98.07N^{0.305}$	Sandy Soil*
		$V_s = 163.15N^{0.192}$	Clayey Soil*
7	[21]	$V_s = 58N^{0.39}$	All Soils*
		$V_s = 73N^{0.33}$	Sandy Soil*
		$V_s = 60N^{0.36}$	Silty Soil*
		$V_s = 44N^{0.48}$	Clayey Soil*
8	[22]	$V_s = 95.64N^{0.301}$	All Soils*
		$V_s = 100.53N^{0.265}$	Sandy Soil*
		$V_s = 89.31N^{0.358}$	Clayey Soil*
9	[23]	$V_s = 105.7N^{0.327}$	All Soils*
		$V_s = 79.7N^{0.365}$	Sandy Soil*
		$V_s = 88.8N^{0.370}$	Clayey Soil*
10	[24]	$V_s = 68.96N^{0.51}$	All Soils*
		$V_s = 60.17N^{0.56}$	Sandy Soil*
		$V_s = 106.63N^{0.39}$	Clayey Soil*
11	[25]	$V_s = 105.03N^{0.286}$	All Soils*
Remarks	From (2000 to 2014)	For the nonlinear power model, $19 \leq a \leq 163.15$ $0.192 \leq b \leq 0.85$	Different types of Soil**

Note: a, b, c, d, e, f, g, h, I, and j are arbitrary constants.

* Nonlinear power model ($Y = a \cdot xb$)

** One model was used which was represented by nonlinear power model



a



b

Fig. 1. The locations of boreholes on the google map (a) borehole No. 1, and (b) borehole No. 2

Table 2

Laboratory and Field Test Results for the Borehole No. 1

BH. No.1	Depth (m)		Index Properties, %			Particle Size Distribution, %				SPT (blow/30 cm)	USCS	USCS Group Name	Strength (kN/m ²) <i>C = q_u/2</i>
	Sample No.	From	To	MC	LL	PI	Clay	Silt	Sand				
1	0	0.5	–	–	–	–	–	–	–	–	–	–	–
2	1	2	17	39	18	36	60	4	0	–	CL	Lean Clay	85
3	2	3	25	41	18	30	64	6	0	–	CL	Lean Clay	75
4	3	3.5	–	–	–	–	–	–	–	13	–	–	–
5	3.5	4.5	–	–	–	–	–	–	–	–	–	–	–
6	4.5	5.5	24	39	18	31	59	10	0	–	CL	Lean Clay	–
7	5.5	6	–	–	–	–	–	–	–	14	–	–	–
8	6	6.5	–	–	–	–	–	–	–	–	–	–	–
9	6.5	7.5	21	41	20	33	56	11	0	–	CL	Lean Clay	140
10	7.5	8.5	–	–	–	–	–	–	–	–	–	–	–
11	8.5	9	–	–	–	–	–	–	–	10	–	–	–
12	9	10	–	43	20	38	55	7	0	–	CL	Lean Clay	–

Table 3

Laboratory and Field Test Results for the Borehole No. 2

BH. No.2	Depth (m)		Index Properties, %			Particle Size Distribution, %				SPT (blow/30 cm)	USCS	USCS Group Name	Strength (kN/m ²) <i>C = q_u/2</i>
	Sample No.	From	To	MC	LL	PI	Clay	Silt	Sand				
1	0	0.5	–	–	–	–	–	–	–	–	–	–	–
2	0.5	1	–	–	–	–	–	–	–	9	CL	Lean Clay	–
3	1	1.5	–	37	17	25	70	5	0	–	CL	Lean Clay	–
4	1.5	2.5	26	39	17	41	53	6	0	–	–	–	110
5	2.5	3.5	27	40	18	44	51	5	0	–	–	–	160
6	3.5	4	–	–	–	–	–	–	–	15	CL	Lean Clay	–
7	4	5	–	–	–	–	–	–	–	–	–	–	–
8	5	6	24	36	16	26	62	12	0	–	–	–	–
9	6	7.5	–	–	–	–	–	–	–	–	CL	Lean Clay	–
10	7.5	8	–	–	–	–	–	–	–	14	–	–	–
11	8	9.5	36	41	21	26	60	12	2	–	–	–	–
12	9.5	10	–	–	–	–	–	–	–	17	CL	Lean Clay	–

Table 4

The results of consolidation test for samples selected from both borehole 1 and 2

BH. No.	Depth (m)		<i>P_o</i> (kN/m ²)	<i>e_o</i>	<i>P_c</i> (kN/m ²)	<i>P_c/P_o</i>	<i>C_c</i>	<i>C_r</i>
	From	To						
1	2	3	48	0.72	103	2.15	0.193	0.034
1	4.5	5.5	73	0.70	105	1.44	0.206	0.025
1	6.5	7.5	93	0.69	108	1.16	0.193	0.028
2	2.5	3.5	53	0.67	106	2.0	0.199	0.035
2	5	6	78	0.65	101	1.29	0.173	0.039

Liquefaction investigation. Normally, the liquefaction is quantified depending on the factor of safety that is expressed in terms of the ratio of the soil resistance against liquefaction (cyclic stresses) divided by the cyclic stresses due to the design earthquake as clearly identified in (3). Normalization with respect to the effective overburden stress for these stress parameters was performed. Both are named as the cyclic resistance and cyclic stress ratios (*CRR* and *CSR*) respectively.

$$F_s = \frac{CRR_{7.5}}{CSR} \cdot K_\sigma \cdot K_\alpha, \quad (3)$$

where F_s is the factor of safety; CSR is the cyclic stress ratio; $CRR_{7.5}$ is the cyclic resistance ratio; K_α is the ground slope correction factor; K_σ is the overburden stress correction factor.

The factor of safety is chosen depending on the significance of the constructed project and the impact of the subsoil

displacement. Both $CRR_{7.5}$ and CSR were computed based on the following:

1. The overburden stress factor K_σ is quantified using the following relationship

$$K_\sigma = \left(\frac{\sigma_{v0}}{P_a} \right)^{f-1},$$

where P_a is the atmospheric pressure compatible in the units with the overburden soil pressure (σ_{v0}); f is a factor that can be calculated depending on the relative soil density (D_r) as follows

$$f = 1 - 0.005 \cdot D_r \quad \text{for } 40\% < D_r < 80\%.$$

2. CRR is typically calculated from field tests such as shear wave velocity values, Becker penetration test, standard penetration test, and cone penetration test. The factor of safety is corrected by a magnitude-scaling factor (MSF) for earthquakes with magnitudes rather than 7.5.

$$F_s = \frac{CRR_{7.5}}{CSR} \cdot MSF,$$

where $CRR_{7.5}$ is the cyclic stress resistance ratio for an earthquake that has a magnitude of 7.5. For MSF evaluation, the following equation was suggested

$$MSF = (7.5/M)^{2.56},$$

where M is the recorded earthquake magnitude.

3. Throughout the previous era, the shear wave velocity was utilized to predict the liquefaction resistance [27]. The shear wave velocity is used for liquefaction resistance because it is similar to CRR being affected by void ratio, effective confining stresses, geological age, and stress history.

A stress-based liquefaction estimation technique depending on collected data from Imperial Valley, California was proposed. The shear wave velocity was normalized as follows

$$V_{s1} = V_s^* \left(\frac{P_a}{\sigma_v} \right)^{0.25},$$

where P_a is the atmospheric pressure (100 kPa); V_{s1} is the standardized shear wave velocity; σ_v is the effective overburden stress. Both shear wave velocity and shear modulus are related directly as follows

$$G_{\max} = \rho \cdot V_s^2, \quad (4)$$

where ρ is the soil density; G_{\max} is the maximum shear modulus.

The average shear modulus (G_{av}) is defined as the division of the average shear stress (τ_{av}) to the average shear strain (γ_{av}).

$$G_{av} = \frac{\tau_{av}}{\gamma_{av}}. \quad (5)$$

For a given shear wave velocity, a cyclic stress ratio (CSR) of a certain magnitude that distinguishes between liquefaction and non-liquefaction instances is called a cyclic stress ratio (CRR). Al-Taie and Albusoda [28] have stated a relationship correlating CSR with shear wave velocity using both (4, 5)

$$CSR = \frac{\tau_{av}}{\sigma_v} = f(\gamma_{av}) v_{s1}^2,$$

where $f(\gamma_{av})$ is dependent on the average shear strain (γ_{av}) since CSR and CRR are equal at the boundary edge identifying the liquefaction and non-liquefaction zones.

The CSR Equation was also modified [27] to

$$CSR = \left[a \cdot \left(\frac{v_{s1}}{100} \right)^2 + b \cdot \left(\frac{1}{v_{s1}^* - v_{s1}} - \frac{1}{v_{s1}^*} \right) \right] \cdot MSF,$$

where v_{s1}^* is the highest limit of v_{s1} for recurring liquefaction incidence, both a and b are the curve fitting parameters, and MSF is the magnitude of the scaling factor. For an earthquake

with a magnitude of 7.5, both a and b are 0.03 and 0.9 respectively. For v_{s1}^* , the following values can be used as summarized in Table 5 [27].

Results and discussion. In Iraq, the seismic activity has changed recently and a great concern has been grown whether the soil formation can sustain such action or not. Northern Iraq experiences acceleration in the range of (0.1 to 0.2 g), according to the map's geodynamic contours [29]. Hence, the soil in such regions might be exposed to liquefaction. With the data on the field-tested soil in two different boreholes, efforts were made to assess the liquefaction using the values of the shear wave velocity as recommended in the literature. In addition, minimum and maximum bounds for the relationship of N values incorporated with shear wave velocity were utilized. The liquefaction was evaluated depending on an earthquake magnitude range from 5.6 to 7.3. These values were chosen because they are comparable to those earthquake values that hit Iraq in the past and have the potential to trigger liquefaction in the future.

Shear Wave Velocity of 210 m/s. Fig. 2 displays the relationship between the cyclic strength ratio (CSR) and depth for the soil condition in borehole 1 (Figs. 2, $a-c$). The CSR was calculated depending on the shear wave velocity of 210 m/s that was recommended in the literature. Generally, the process of liquefaction is related to the geotechnical soil properties and seismic characteristics. Thus, the results of Figs. 2, $a-c$ indicate that the CSR increases with the depth where the soil is not exposed to liquefaction along the depth in most of the cases. However, the only observed range of liquefaction can be noticed between the depth of 6 to 9 m when $M=7.3$ and $a=0.24$ g (Fig. 2, c). As the depth increases from 3.5 to 6 m, the CSR increases by 21%. In addition, the CSR increases by 32% as the depth increases from 3.5 to 9 m.

Similarly, Fig. 2 shows the depth-dependent variation of the cyclic strength ratio (CSR) for the soil characteristics in borehole 2 (Figs. 2, $d-f$). The CSR was calculated depending on the shear wave velocity of 210 m/s that was recommended in the literature. The results of Figs. 2, $d-f$ indicate that the CSR increases with the depth where the soil is not exposed to liquefaction along the depth in all the studied cases. As the depth increases from 1 to 4 m, the CSR increases by 12%. In addition, the CSR increases by 37 and 40% as the depth increases from 1 to 8 m and 1 to 10 m respectively.

Both CSR and CRR measurements are used to make predictions about the safety factor. When the safety factor is less than 1, liquefaction can occur at any depth. Thus, the results of Figs. 3, $a-c$ show that the factor of safety in borehole 1 is decreased with the depth where the soil is not exposed to failure along the depth in most of the studied cases. However, the only observed range of failure can be remarked between the depth of 6 to 9 m when $M=7.3$ and $a=0.24$ g (Fig. 3, c). As the depth increases from 3.5 to 6 m, the factor of safety for the worst-case scenario decreases by 25%. In addition, the factor of safety decreases by 94% in the worst-case scenario as the depth increases from 3.5 to 9 m. As the M value increases from 5.6 to 7.3, the factor of safety decreases by 49%. However, the factor of safety decreased by 38% as the acceleration value increases from 0.15 to 0.24.

Figs. 3, $d-f$ likewise displays the data for borehole 2, showing how the safety factor varies with depth. In all situations

Table 5

The values of upper limits of shear wave velocity with soil type [27]

v_{s1}^* , m/s	Soil type	Fine content, %
220	Sands and gravels	<5
210	Sands and gravels	≈20
200	Sands and gravels	>35

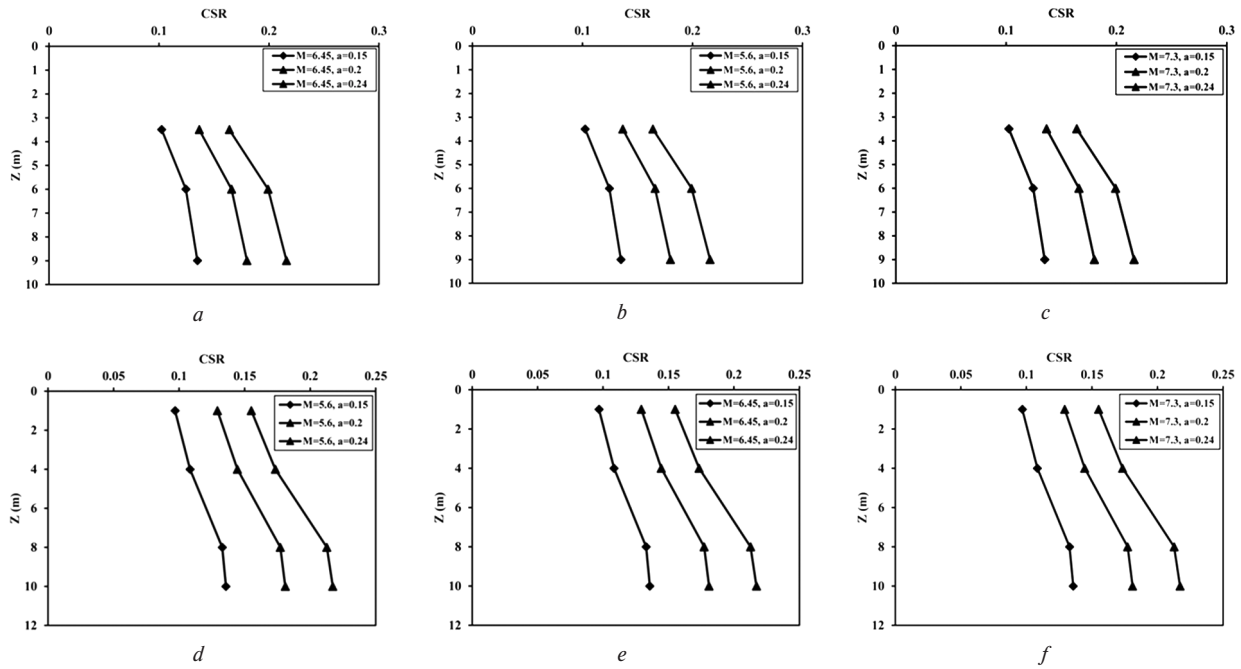


Fig. 2. The variation of CSR with the depth:

a – BH1, $M = 5.6$; b – BH1, $M = 6.45$; c – BH1, $M = 7.3$; d – BH2, $M = 5.6$; e – BH2, $M = 6.45$; f – BH2, $M = 7.3$

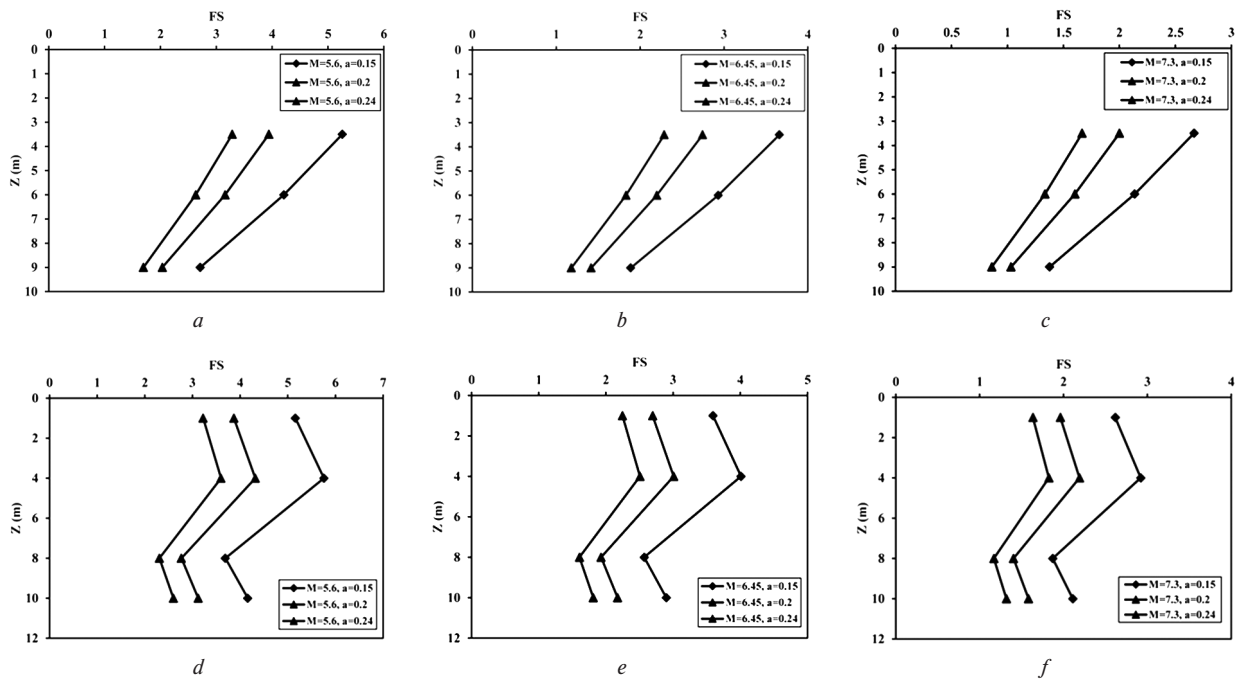


Fig. 3. The variation of FS with the depth:

a – BH1, $M = 5.6$; b – BH1, $M = 6.45$; c – BH1, $M = 7.3$; d – BH2, $M = 5.6$; e – BH2, $M = 6.45$; f – BH2, $M = 7.3$

where the factor of safety was greater than one, the soil was found to be safe against liquefaction. As the depth increases from 1 to 4 m (in the worst-case scenario represented by Fig. 3, f), the factor of safety increased by 12%. Nevertheless, the factor of safety for the same worst-case scenario decreases by 28 and 19% as the depth increases from 1 to 8 m and 1 to 10 m respectively.

Shear Wave versus N . Table 1 shows that for various soil types, there are various mathematical correlations between shear wave velocity and N values. Figs. 4, a–d illustrates the variations in shear wave velocity at varying N values for all soil types, sand, silt, and clay. It is clearly shown the shear wave velocity increases nonlinearly with increasing N values for various types of soil. The range of shear wave velocities is

shown to vary with N levels for all soil types in Fig. 5. The field measured values for the N in both boreholes 1 and 2 range from 9 to 17. Thus, the bounds on the variation of shear wave velocity with N values to simulate the real field data may be represented by both (6, 7).

$$\text{Lower Limit: } V_s = 68.3 \cdot N^{0.292}, \quad (6)$$

$$\text{Upper Limit: } V_s = 106.63 \cdot N^{0.39}. \quad (7)$$

Lower Limit. Figs. 6, a–c displays the depth dependence of the cyclic strength ratio (CSR) for the soil condition in borehole 1. The CSR has been calculated depending on the lower limit of the shear wave velocity that is given by (6). The results of Figs. 6, a–c indicate that the CSR increases with the depth

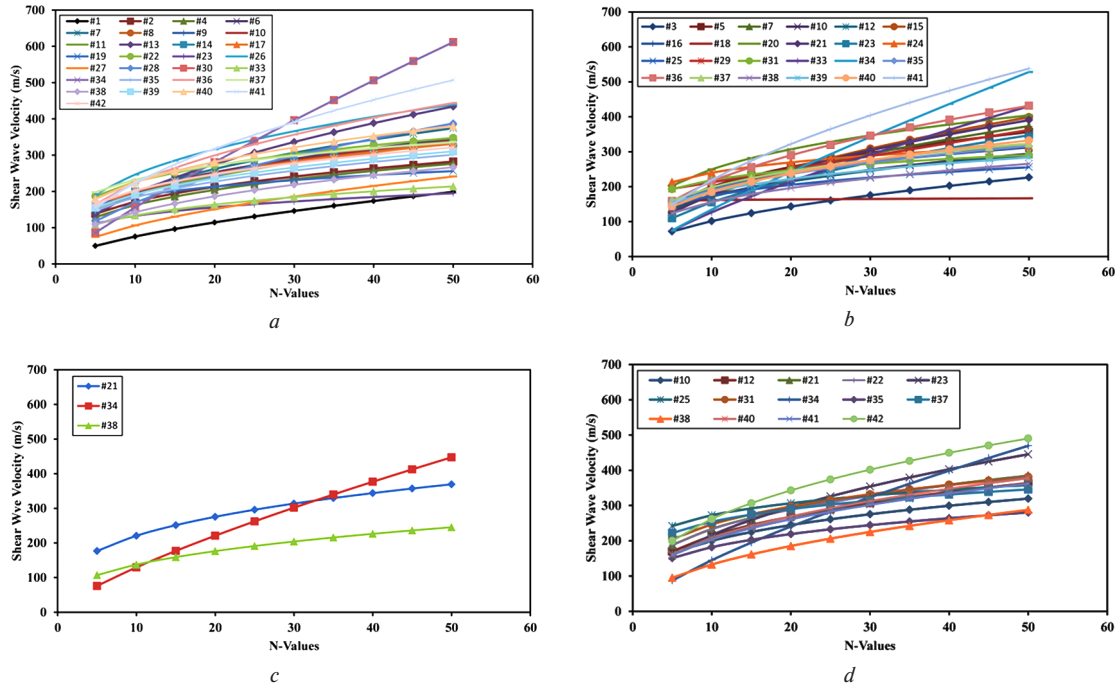


Fig. 4. The variation of shear wave velocity with N values:
 a – all soil types; b – sandy soil type; c – silty soil type; d – clayey soil type

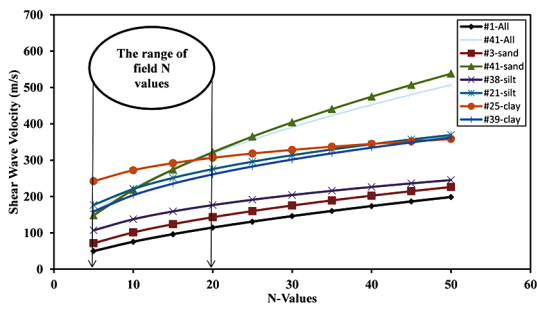


Fig. 5. The variation of upper and lower limits of shear wave velocity with N values for all soil types

where the soil is exposed to liquefaction along the depth in all the studied cases. As the depth increases from 3.5 to 6 m, the CSR increases by 21%. In addition, the CSR increases by 32% as the depth increases from 3.5 to 9 m.

Figs. 6, $d-f$ displays the depth-dependent change in the cyclic strength ratio (CSR) for the soil condition in borehole 2. The CSR was calculated depending on the lower limit of the shear wave velocity that is given by (6). The results of Figs. 6, $d-f$ indicate that the CSR increases with the depth where the soil is exposed to liquefaction along all the depths in all the studied cases. As the depth increases from 1 to 4 m, the CSR increases by 12%. In addition, the CSR increases by 37 and 40% as the depth increases from 1 to 8 m and 1 to 10 m respectively.

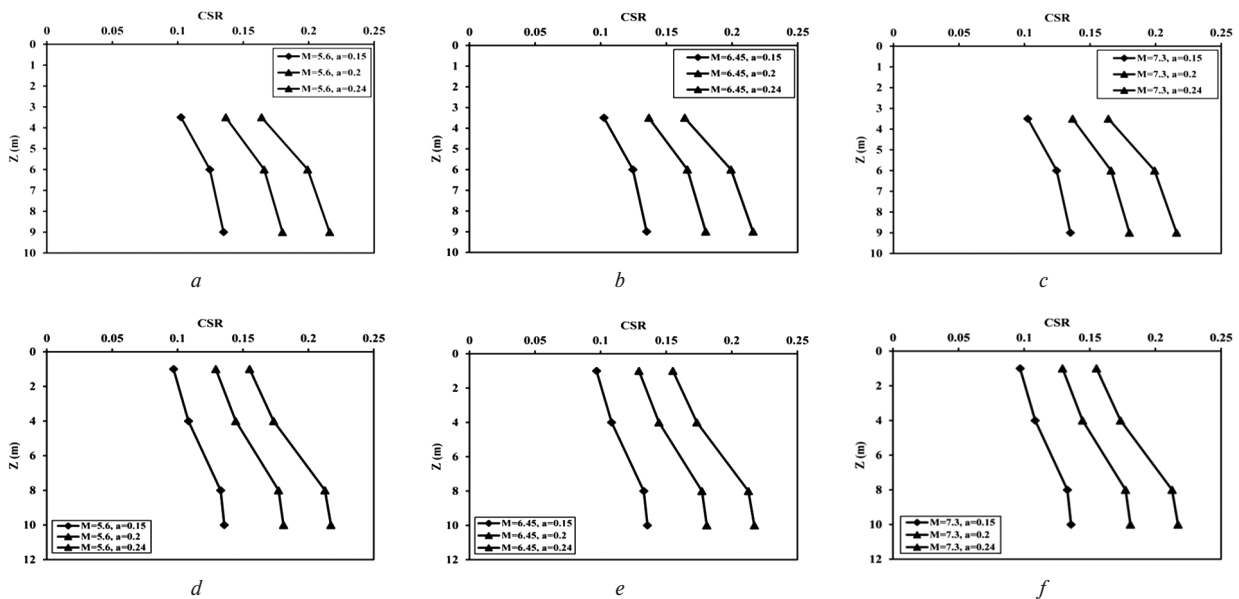


Fig. 6. The variation of CSR with the depth using lower limit relationship:
 a – BH1, $M = 5.6$; b – BH1, $M = 6.45$; c – BH1, $M = 7.3$; d – BH2, $M = 5.6$; e – BH2, $M = 6.45$; f – BH2, $M = 7.3$

The factor of safety is predicted using both *CSR* and *CRR* values depending on the lower limit of shear wave velocity relationship (6). The results of Figs. 7, *a–c* show that the factor of safety in borehole 1 decreases with the depth where the soil is subjected to failure along the depth in all the investigated cases. As the depth increases from 3.5 to 6 m, the factor of safety for the worst-case scenario decreases by 24 %. It is also worth noting that going from 3.5 to 9 m deep reduces the safety factor by 59 % (in the worst case).

On the other hand, the results of Figs. 7, *d–f* present the variation of the factor of safety with the depth of the borehole 2. When evaluating the risk of liquefaction, the results show that in every scenario analyzed, the safety factor is less than one, indicating that the soil is dangerous. As the depth increases from 1 to 4 m (in the worst-case scenario represented by Fig. 7, *f*), the factor of safety decreases by 12 %. Moreover, the factor of safety for the same worst-case scenario decreases by 47 and 40 % as the depth is increased from 1 to 8 m and 1 to 10 m respectively.

Upper limit. Fig. 8 displays the depth-dependent variation in the cyclic strength ratio (*CSR*) for the soil condition in borehole 1. The *CSR* was calculated depending on the maximum limit of the shear wave velocity that is given by (7). The results of Figs. 8, *a–c* indicate that the *CSR* increases with the depth where the soil is not exposed to liquefaction along the depth in most of the studied cases. Nevertheless, the liquefaction zone can be noticed between the depth 6 to 9 m when $a \geq 0.2$ and $M \geq 6.45$. As the depth increases from 3.5 to 6 m, the *CSR* increases by 21 %. In addition, the *CSR* increases by 32 % as the depth increases from 3.5 to 9 m.

Figs. 8, *d–f* also displays the depth-dependent change in the cyclic strength ratio (*CSR*) for the soil condition in borehole 2. The *CSR* was calculated depending on the upper limit of the shear wave velocity that is given by (7). The results of Figs. 8, *d–f* indicate that the *CSR* increases with the depth where the soil is not exposed to liquefaction along most of the depths for all the studied cases. Nevertheless, the liquefaction zone can be noticed between the depth of 4 to 10 m when $a \geq$

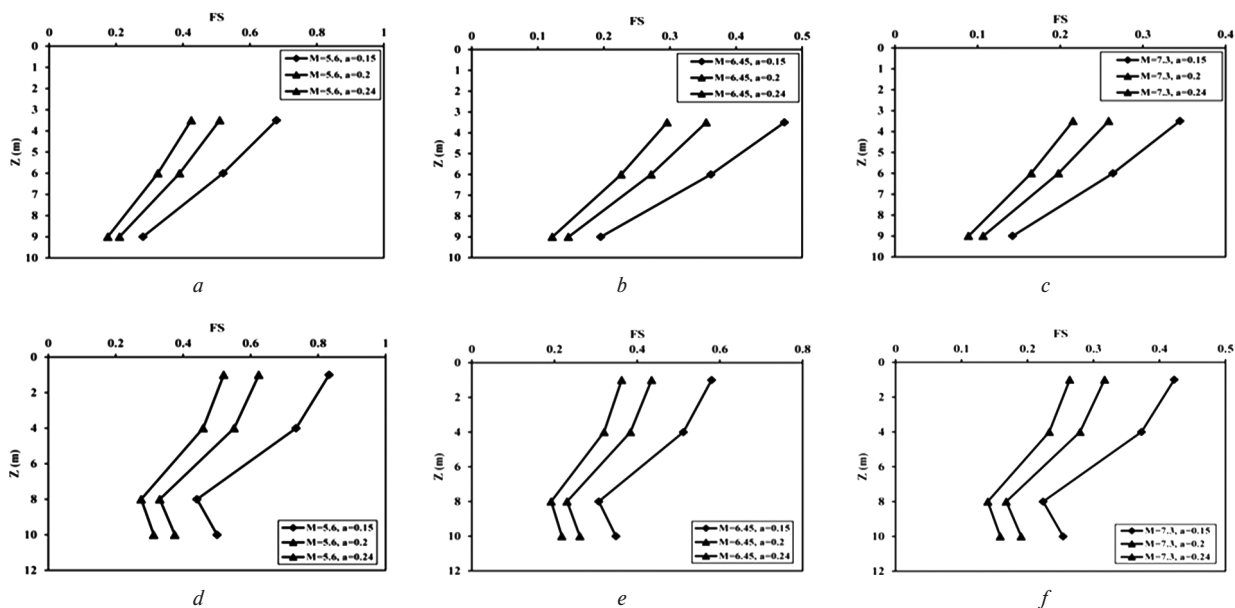


Fig. 7. The variation of FS with the depth using lower limit relationship:

a – BH1, $M = 5.6$; *b* – BH1, $M = 6.45$; *c* – BH1, $M = 7.3$; *d* – BH2, $M = 5.6$; *e* – BH2, $M = 6.45$; *f* – BH2, $M = 7.3$

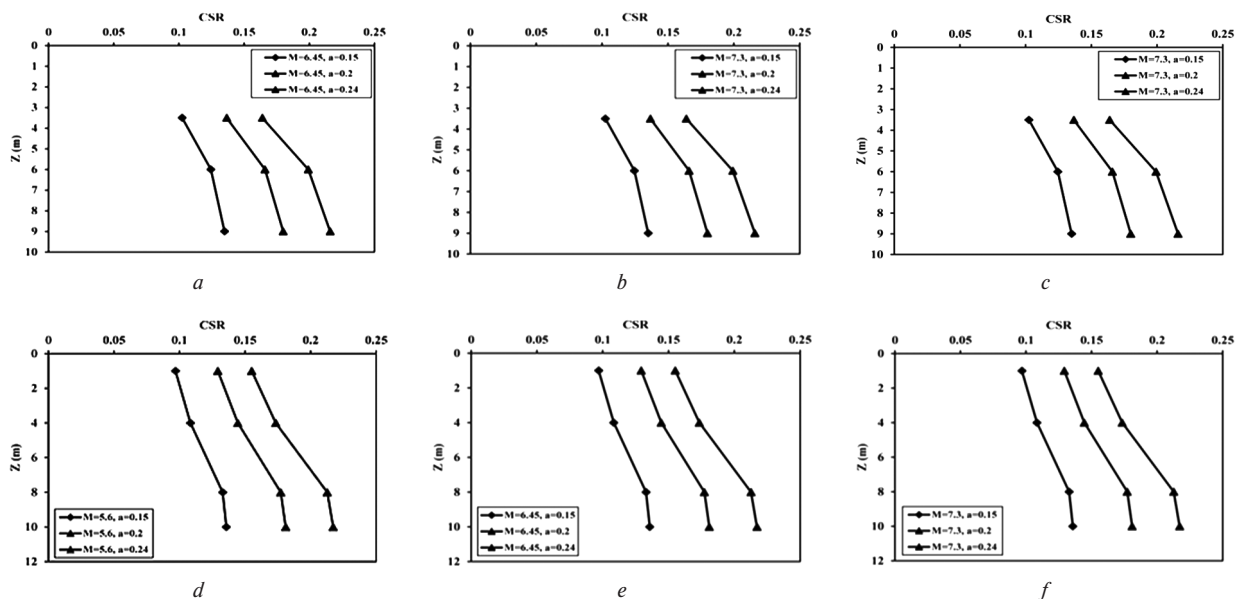


Fig. 8. The variation of CSR with the depth using upper limit relationship:

a – BH1, $M = 5.6$; *b* – BH1, $M = 6.45$; *c* – BH1, $M = 7.3$; *d* – BH2, $M = 5.6$; *e* – BH2, $M = 6.45$; *f* – BH2, $M = 7.3$

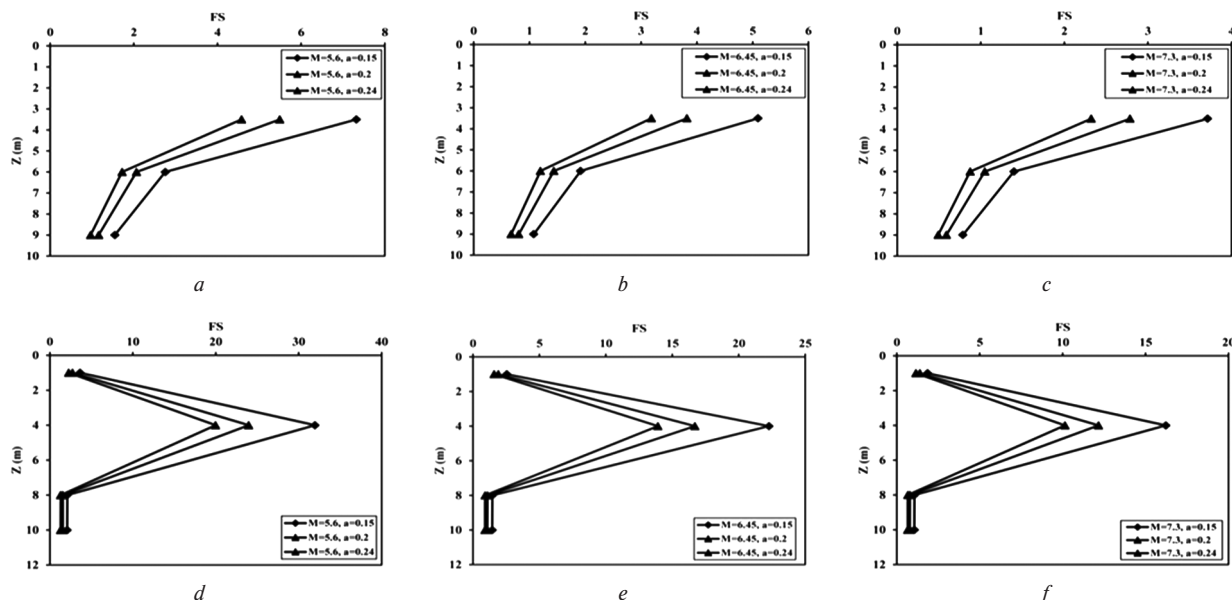


Fig. 9. The variation of FS with the depth using upper limit relationship:

a – BH1, $M = 5.6$; b – BH1, $M = 6.45$; c – BH1, $M = 7.3$; d – BH2, $M = 5.6$; e – BH2, $M = 6.45$; f – BH2, $M = 7.3$

≥ 0.24 and $M \geq 6.45$. As the depth increases from 1 to 4 m, the CSR increases by 12 %. In addition, the CSR increases by 37 and 40 % as the depth increases from 1 to 8 m and 1 to 10 m respectively. The factor of safety is predicted using both CSR and CRR values depending on the upper limit of the shear wave velocity relationship (7). The results of Figs. 9, a–c demonstrate that for all analyzed scenarios, the safety factor in borehole 1 decreases with increasing depths where the soil is susceptible to collapse. As the depth increases from 3.5 to 6 m, the factor of safety for the worst-case scenario decreases by 62 %. In addition, the factor of safety decreases by 79 % for the worst-case scenario as the depth increases from 3.5 to 9 m.

Alternatively, the results of Figs. 9, d–f present the variation of the factor of safety with the depth of the borehole 2. The results indicate that the soil is safe in most of the studied cases in terms of liquefaction as the factor of safety is higher than one. When the depth increases from 1 to 4 m for the worst-case scenario represented by Fig. 9, f, the factor of safety increases by 776 %. Nevertheless, the factor of safety for the same worst-case scenario decreases by 43 % whether the depth increases from 1 to 8 m or 1 to 10 m.

As an overall site evaluation, there are chances to have liquefaction at deeper depths because of the existence of weak soil stratum at higher depths. This can be remarked from the field N-SPT values for both boreholes that have lower values at higher depths. Consequently, precautions and possible site protections are required.

Conclusions. Liquefaction evaluation of the Kirkuk city industrial zone utilizing two practical field borehole data has been investigated in this study. The shear wave velocity was calculated using recommended values from the literature. In addition, lower and upper limits for the relation of the shear wave velocity versus N values were used. From the outcomes of the present study, the subsequent findings were advanced:

The Kirkuk soil at the industrial zone is susceptible to liquefaction between the depths of 6 and 9 m using the recommended shear wave velocity when $M = 7.3$ and $a = 0.24g$.

For the used shear wave velocity, the earthquake magnitude has more effect on liquefaction potential in comparison with the acceleration value.

As the depth is extended from 3.5 to 9 m, the factor of safety decreases by 94 % when the worst-case scenario and the recommended shear wave velocity were used.

In the worst-case state and depending on the recommended shear wave velocity, the only observed range of failure can

be remarked between the depth of 6 to 9 m when $M = 7.3$ and $a = 0.24g$.

Generally, it was observed that the liquefaction depth increases with increasing the ground acceleration.

As a result, the soil in Kirkuk industrial zone is vulnerable to liquefaction along the depth for the lower limit of the shear wave velocity in all the analyzed instances.

The soil fails along its depth for the minimum shear wave velocity in all of the studied scenarios.

Kirkuk soil in the industrial zone is not vulnerable to liquefaction along the depth for the examined highest shear wave velocities.

For the highest limit of the shear wave velocity, the soil is subjected to failure along several depths for all the investigated cases.

References.

1. Tabatabaei, S.A., Esmaceli, M., & Sadeghi, J. (2019). Investigation of optimum height of railway embankments during earthquake based on their stability in liquefaction. *Journal of Earthquake Engineering*, 23(5), 882-908. <https://doi.org/10.1080/13632469.2017.1342301>.
2. Fattah, M. Y., Al-Neami, M. A., & Jajjawi, N. H. (2014). Prediction of Liquefaction Potential and Pore Water Pressure beneath Machine Foundations. *Central European Journal of Engineering*, 4(3), 226-249. <https://doi.org/10.2478/s13531-013-0165-y>.
3. Fattah, M. Y., Salim, N. M., & Haleel, R. J. (2018). Liquefaction Potential of Sandy Soil from Small Laboratory Machine Foundation Model. *International Review of Civil Engineering*, 9(1), 11-19. <https://doi.org/10.15866/irece.v9i1.13737>.
4. Abdullah, H. H., Fattah, M. Y., & Abed, A. H. (2018). Determination of Liquefaction Potential for Two Selected Sites in Kerbala City-Middle of Iraq. *International Journal of Engineering & Technology*, 7(1), 25-32. <https://doi.org/10.14419/ijet.v7i1.8268>.
5. Ecemis, N. (2020). Effect of soil-type and fines content on liquefaction resistance-shear wave velocity correlation. *Journal of Earthquake Engineering*, 24(8), 1311-1335. <https://doi.org/10.1080/13632469.2018.1475312>.
6. Karim, H. H., Fattah, M. Y., & Hasan, A. M. (2010). Evaluation of Some Geotechnical Properties and Liquefaction Potential from Seismic Parameters. *Iraqi Journal of Civil Engineering*, 6(3), 30-45.
7. Tong, L., Che, H., Pan, H., Zhang, M., & Guo, Q. (2019). Comparison of shear wave velocity prediction models to Yangtze river deltaic sediments based on piezocone test data. *International Journal of Civil Engineering*, 17, 1845-1858. <https://doi.org/10.1007/s40999-019-00408-3>.
8. Karray, M., Lefebvre, G., Ethier, Y., & Bigras, A. (2011). Influence of particle size on the correlation between shear wave velocity and cone tip resistance. *Canadian Geotechnical Journal*, 48(4), 599-615. <https://doi.org/10.1139/t10-092>.

9. Chen, Y.R., Chen, J.W., Shun-Chieh Hsieh, S.C., & Chang, Y.T. (2013). Evaluation of soil liquefaction potential based on the nonlinear energy dissipation principles. *Journal of Earthquake Engineering*, (17), 54-72. <https://doi.org/10.1080/13632469.2012.691256>.

10. Kasim, M. N., & Raheem, A. M. (2021). Evaluation of some soil characteristics from field SPT values using random number generation technique. *IOP Conference Series: Earth and Environmental Science*, (779), 012017, 2-13. <https://doi.org/10.1088/1755-1315/779/1/012017>.

11. Wichtmann, T., & Triantafyllidis, T. H. (2009). Influence of the grain size distribution curve of quartz sand on the small strain shear modulus Gmax. *Journal of Geotechnical and Geoenvironmental Engineering ASCE*, 135(10), 1404-1418. [https://doi.org/10.1061/\(ASCE\)GT.1943-5606.0000096](https://doi.org/10.1061/(ASCE)GT.1943-5606.0000096).

12. Bui, M. T., Clayton, C. R. I., & Priest, J. A. (2007). Effects of particle shape on Gmax of geomaterials. *Earthquake Geotechnical Engineering*, 1536.

13. Santamarina, J. C., Klein, A., & Fam, M. A. (2001). Soils and waves: Particulate materials behavior, characterization and process monitoring. *Journal of Soils and Sediments*, 1(2), 130. <https://doi.org/10.1007/BF02987719>.

14. Yimsiri, S., & Soga, K. (2000). Micromechanics-based stress-strain behaviour of soils at small strains. *Geotechnique*, 50(5), 559-571. <https://doi.org/10.1680/geot.2000.50.5.559>.

15. Chien, L. K., Lin, M. C., & Oh, E. (2000). Shear wave velocity evaluation on reclaimed soil in West Taiwan. *International Journal of Offshore and Polar Engineering*, 10(1), 73-79.

16. Kiku, H., Yoshida, N., Yasuda, S., Irisawa, T., Nakazawa, H., Shimizu, Y., Ansal, A., & Erkan, A. (2001). In-situ penetration tests and soil profiling in Adapazari, Turkey. *Proceedings of the ICSMGE/TC4 satellite conference on lessons learned from recent strong earthquakes*, 259-265. Retrieved from <https://cir.nii.ac.jp/crid/1573387449937537280>.

17. Jafari, M. K., Shafiee, A., & Razmkhah, A. (2002). Dynamic properties of fine grained soils in the south of Tehran. *Journal of Seismological Earthquake Engineering*, 4(1), 25-35.

18. Hasancebi, N., & Ulusay, R. (2007). Empirical correlations between shear wave velocity and penetration resistance for ground shaking assessments. *Bulletin of Engineering Geology and the Environment*, (66), 203-213. <https://doi.org/10.1007/s10064-006-0063-0>.

19. Hanumantharao, C., & Ramana, G. V. (2008). Dynamic soil properties for microzonation of Delhi, India. *Journal of Earth System Science*, 117(S2), 719-730. <https://doi.org/10.1007/s12040-008-0066-2>.

20. Lee, C. T., & Tsai, B. R. (2008). Mapping Vs30 in Taiwan. *Terrestrial, Atmospheric and Oceanic Sciences*, 19(6), 671-682. [https://doi.org/10.3319/TAO.2008.19.6.671\(PT\)](https://doi.org/10.3319/TAO.2008.19.6.671(PT)).

21. Dikmen, U. (2009). Statistical correlations of shear wave velocity and penetration resistance for soils. *Journal of Geophysics and Engineering*, 6(1), 61-72. <https://doi.org/10.1088/1742-2132/6/1/007>.

22. Uma Maheswari, R., Boominathan, A., & Dodagoudar, G. R. (2009). Use of Surface Waves in Statistical Correlations of Shear Wave Velocity and Penetration Resistance of Chennai Soils. *Geotechnical and Geological Engineering*, 28(2), 119-137. <https://doi.org/10.1007/s10706-009-9285-9>.

23. Tsiambaos, G., & Sabatakakis, N. (2010). Empirical estimation of shear wave velocity from in situ tests on soil formations in Greece. *Bulletin of Engineering Geology and the Environment*, 70(2), 291-297. <https://doi.org/10.1007/s10064-010-0324-9>.

24. Anbazhagan, P., Kumar, A., & Sitharam, T. G. (2012). Seismic Site Classification and Correlation between Standard Penetration Test N Value and Shear Wave Velocity for Lucknow City in Indo-Gangetic Basin. *Pure and Applied Geophysics*, 170(3), 299-318. <https://doi.org/10.1007/s00024-012-0525-1>.

25. Fauzi, A., Irsyam, M., & Fauzi, U. J. (2014). Empirical correlation of shear wave velocity and N-SPT value for Jakarta. *International Journal of Geomate*, 7(1), 980-984. <https://doi.org/10.21660/2014.13.3263>.

26. Al-Ghuri, H. F., Al-Tawash, B. S., Al-Tamimi, O. S., & Schüth, C. (2023). Impacts of hydrogeochemical processes and land use practices on groundwater quality of Shwan sub-Basin, Kirkuk, northern Iraq. *Heliyon*, 9(3), e13995. <https://doi.org/10.1016/j.heliyon.2023.e13995>.

27. Andrus, R. D., & Stokoe II, K. H. (2000). Liquefaction Resistance of Soils from Shear-Wave Velocity. *Journal of Geotechnical and Geoen-*

vironmental Engineering, 126(11), 1015-1025. [https://doi.org/10.1061/\(asce\)1090-0241\(2000\)126:11\(1015\)](https://doi.org/10.1061/(asce)1090-0241(2000)126:11(1015)).

28. Al-Taie, A. J., & Albusoda, B. S. (2019). Earthquake hazard on Iraqi soil: Halabjah earthquake as a case study. *Geodesy and Geodynamics*, (10), 196-204. <https://doi.org/10.1016/j.geog.2019.03.004>.

29. Jassim, S. Z., & Goff, J. C. (2006). *Geology of Iraq*. Dolin, Prague and Moravian Museum, Brno, Czech Republic. ISBN: 80-7028-287-8.

Розрідження промислової зони від сейсмічних навантажень із використанням лабораторних і польових вимірювань

Арам Мохаммед Рахім*

Кафедра цивільного будівництва, Кіркукський університет, м. Кіркук, Ірак

* Автор-кореспондент: e-mail: aram_raheem@uokirkuk.edu.iq

Мета. Оцінити розрідження промислового регіону Кіркука після серії землетрусів, що сталися в місті протягом попередніх п'яти років, на основі поточної сейсмічної активності в регіоні.

Методика. Спочатку були зібрані й вивчені суттєві залежності швидкості зсувних хвиль у різних типах ґрунтів, причому більшість із цих залежностей вимагали використання стандартних випробувань на прохідність у польових умовах. Фактично були пробурені дві свердловини на максимальну глибину 10 м, а кількість ударних хвиль при проведенні стандартних випробувань на прохідність вимірювалася на різних глибинах у кожній свердловині. Використовувалася базова методика на основі літературних значень швидкості зсувної хвилі, а також максимальної й мінімальної швидкості зсувної хвилі для оцінки циклічного напруження зсуву, викликаного сейсмічним навантаженням.

Результати. На основі лабораторних і польових даних можна визначити запаси стійкості до розрідження, спричиненого землетрусом. При розгляді найгіршого сценарію з використанням запропонованих значень швидкості зсувних хвиль, коефіцієнт стійкості до землетрусу зменшився на 94 % при збільшенні глибини з 3,5 до 9 м.

Наукова новизна. Жодне попереднє дослідження не було спрямоване на кількісну оцінку впливу розрідження на промислову зону міста Кіркук, оскільки така важлива багата на нафту територія зазнала впливу серії землетрусів. Що більш важливо, уперше були зібрані й використані для оцінки розрідження польові зразки ґрунту зі свердловин у місті Кіркук, оскільки такі актуальні польові дані можуть бути належним чином використані у процесі оцінки розрідження за умови відсутності будь-якої порівняльної кількісної оцінки на досліджуваній ділянці.

Практична значимість. До початку будівництва будь-якого запропонованого проекту у світлі підвищеної сейсмічної активності у промисловій зоні міста Кіркук (Ірак) слід проводити аналіз розрідження території розміщення корисних копалин.

Ключові слова: розрідження, випробування на прохідність, землетрус, швидкість зсувних хвиль, порушення ґрунту, коефіцієнт запасу міцності

The manuscript was submitted 09.06.23.